Supporting Information

Supported microwires for electroanalysis: sensitive amperometric detection of reduced glutathione

Kamonwad Ngamchuea, Chuhong Lin, Christopher Batchelor-McAuley, Richard G. Compton*

* corresponding author: Richard G. Compton, Department of Chemistry, Physical & Theoretical Chemistry Laboratory, University of Oxford, South Parks Road, Oxford, OX1 3QZ, United Kingdom

Email: richard.compton@chem.ox.ac.uk. Tel: +44(0)1865275 957 Fax: +44(0)1865275410

S 1 Electrode set-ups

All electrochemical measurements were conducted using standard three electrode setups employing different working electrodes in order to compare the voltammetric responses obtained at electrodes of different geometry. The different set-ups used are summarized in Table S1 below.

Table S1: The different three-electrode setups used in electrochemical measurements

Working electrode		Reference electrode	Counter electrode
Material	**Diameter**		
glassy carbon (CH Instruments)	3 mm	saturated calomel (BASi)	platinum mesh
carboxyl functionalised multi-walled carbon nanotube screen-printed (Dropsens)	4 mm	silver wire	carbon
micro carbon fiber (microdisk, ALS)	7 µm	saturated calomel (BASi)	platinum mesh
Fabricated surface-mounted carbon microwire	7 µm	**$FcCH_2OH$ experiments:** saturated calomel (BASi)	tinned copper wire
		GSH/TNB experiments: silver wire	

S 2 Results and discussions

The simulation and experimental results of a reversible one-electron transfer process (i.e. ferrocenemethanol oxidation) are discussed herein in more details. Further numerical results are also provided for cyclic voltammetry of an irreversible one-electron transfer system at the isolated and surface-mounted microwire electrodes. Raw data of the reproducibility of the length and voltammetric responses of the supported microwire electrodes are also provided. This section ends with the use of chronoamperometry at the supported microwire to qauntitatively detect GSH.

S 2.1 Chronoamperometry

Herein, chronoamperometry of a reversible one-electron transfer process is discussed in more detail including the concentration profiles of a reactant at short and long transient times. The detail of the fitting of experimental results to simulation are also provided.

S 2.1.1 Theory

The main text provides the concentration profiles as a result of cyclic voltammetry of a redox-active species showing the conversion of linear diffusion at very fast scan rates (Fig. 5c) to radial diffusion at slow scan rates (Fig. 5d). In this Supporting Information, we present the concentration profiles of a redox-active species as a result of chronoamperometry at short and long experimental times to show that the results are in agreement with the voltammetry results and further emphasize on the transition from linear to convergent diffusion.

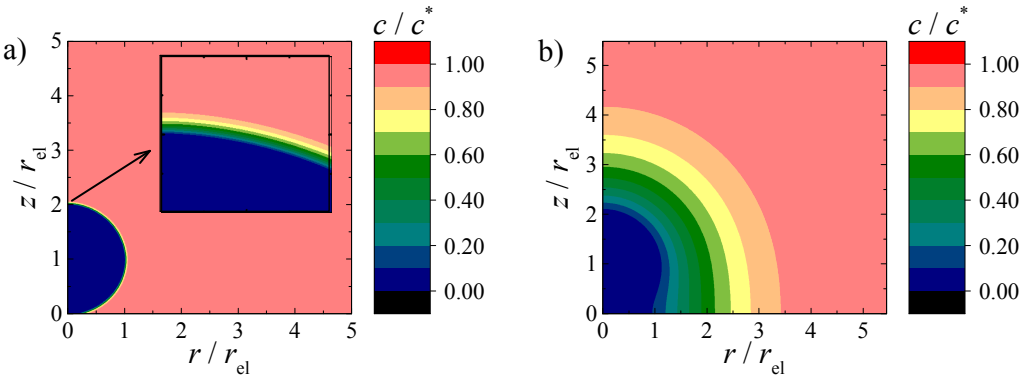

Figure S1: Simulated concentration profiles of the reactant on the supported microcylinder electrode at a) short experimental time ($Dt/r_{el}^2 = 0.1$) and b) long experimental time ($Dt/r_{el}^2 = 100$).

It is known that the diffusion of the reactant from the bulk solution to both the isolated microcylinder and the hemi-microcylinder is isotropic. However, for the supported microcylinder electrode, due to the obstruction of the inert substrate, the bottom of the electrode surface is not fully accessible to the diffusion of the reactant. Two example concentration profiles for the one-electron-transfer reaction on the supported microcylinder at $Dt / r_{el}^2 = 0.1$ and $Dt / r_{el}^2 = 100$ are illustrated in Figure S1a and S1b, respectively. At the beginning of the reaction, as shown in Figure S1a, the size of the diffusion layer is relatively small comparing with the size of the electrode. The diffusion profile is almost linear on the supported microcylinder electrode, in which case the current response from the microcylinder is proportional to the electrode surface area. However, with the reaction time increasing, the influence of the geometry appears as shown in Figure S1b. Due to the block of the substrate, the diffusion to the bottom of the electrode surface is limited and the diffusion layer shows the feature between a hemi-microcylinder and an isolated microcylinder.

S 2.1.2 Experiment

The chronoamperograms of 1.0 mM $FcCH_2OH$ oxidation at the supported microwires are obtained and already discussed in the main text. The experimental data are then compared with the results of numerical simulation. In order to consider comparatively both the linear (1D) and radial (2D) diffusion regimes, as well as to avoid the influence of convective force, the correlation between the simulated and experimental data is studied at short transient times, as further described below.

At transient time (t) of less than 0.3 s, there is a significant non-Faradaic contribution due to the build-up of charged species at the electrode as can be seen from the chronoamperogram of 0.1 M KCl solution where the potential of 0.35 V vs. SCE is applied at the supported microwire (Fig. S2). Consequently, t = 0.3 s was used as the short-time limit (t_{min}) for fitting of experimental data to simulation results. The long-time limit (t_{max}) required for the closest fit is determined by calculating the values of %MSAD (eqn. S1). The long-time limit which gives the lowest %MSAD is chosen for the fitting.

$$\%\mathrm{MSAD} = \frac{1}{N}\sum_N \left|\frac{I_{\mathrm{sim}} - I_{\mathrm{exp}}}{I_{\mathrm{exp}}}\right| \times 100 \qquad \text{(S1)}$$

Figure S3a shows that t_{max} of 3.8 s gives the lowest value of %MSAD of 0.31%. Consequently, the experimental time period of 0.3 s – 3.8 s is chosen as the optimal transient times for the fitting between experimental and simulated results.

As also mentioned in the main text, the concentration of ferrocence methanol and the radius of the electrode are precisely known to be 1.02 mM and 3.5 μm respectively. There are however two unknown parameters, D and l, which are to be determined using %MSAD. The values of D and l which yield the lowest %MSAD of 0.31% are 7.81×10^{-10} m^2 s^{-1} and 1.034 cm respectively; see Fig. S3b.

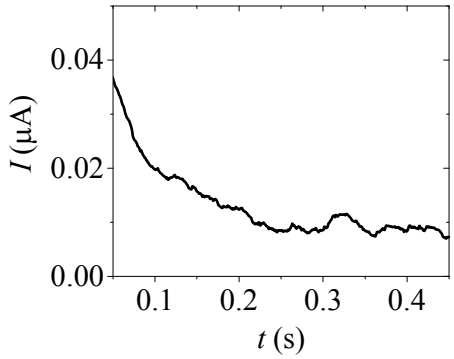

Figure S2: Chronoamperogram of 0.1 M KCl electrolyte solution; E = 0.35 V vs. SCE showing significant contribution from non-Faradaic currents at the experimental time of less than 0.3 s.

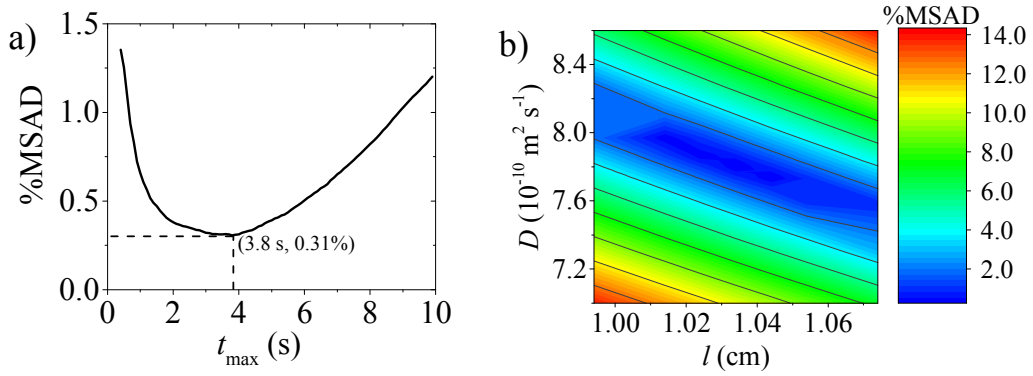

Figure S3: a) %MSAD as a function of long-time limits (t_{max}) showing a minimum of %MSAD of 0.31% when t_{max} is 3.8 s; b) %MSAD as a function of diffusion coefficient (D) and length of the supported wire electrode (l) showing a minimum of %MSAD of 0.29% when D and l are 3.8 s 7.81×10^{-10} m^2 s^{-1} and 1.034 cm respectively.

Having determined the optimal transient times (0.3 s – 3.8 s) for the fitting of the simulated and experimental results, and the values of all the parameters required for the calculation of the current-time responses (c^*, r_{el}, D and l; eqn. 5 in the main text), the simulated and experimental chronoamperograms can then be compared as presented in Fig. S4 below.

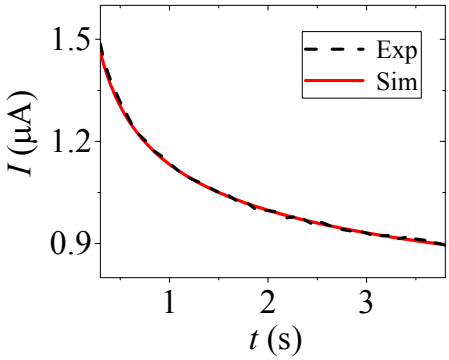

Figure S4: Comparison between the experimental (black, dashed line) and simulated (red, solid line) chronoamperograms of 1.0 mM $FcCH_2OH$ (+0.1 M KCl) oxidation, ν = 25 - 400 mV s^{-1}, 298 K at the supported microcylinder electrode.

S 2.2 Cyclic Voltammetry: Theory

Cyclic voltammetry of a reversible one-electron transfer process (i.e. ferrocenemethanol oxidation) has been discussed regarding the effect of electrode geometry on the electrochemical responses. The $I_{p,supported}$ / $I_{p,isolated}$ ratios are presented as a working curve as a function of $\log_{10}(Fvr_{el}^2/RTD)$ in Fig. 4b, the exact values of which are provided in Table S2. Similar simulation results for an irreversible one-electron transfer process are also discussed below.

S 2.2.1 Reversible electron-transfer

Table S2: The $I_{p,supported}$ / $I_{p,isolated}$ ratios for reversible one-electron transfer process at different Fr_{el}^2v/RTD

$\log_{10}(Fr_{el}^2v/RTD)$	$I_{p,supported}/I_{p,isolated}$
-3.91	0.545
-3.41	0.550
-2.91	0.560
-2.41	0.574
-1.91	0.590
-1.41	0.608
-0.91	0.628
-0.41	0.654
0.09	0.686
0.59	0.724
1.09	0.765
1.59	0.804
2.09	0.838
2.59	0.863
3.09	0.888

S 2.2.2 Irreversible electron-transfer

Similar to Fig. 5b in the main text, the geometry influence on the supported microwire electrode for an irreversible reaction is also explored under different diffusion conditions, referred by the combined parameter Fvr_{el}^2/RTD. Fig. S5 shows the working curve of the $I_{p,supported}$ / $I_{p,isolated}$ ratios as a function of $\log_{10}(Fvr_{el}^2/RTD)$ and the exact values are listed in Table S3 for reference. The peak currents used below are collected from numerical simulation. Different from the reversible case discussed in the main text, for the irreversible one-electron transfer reaction, the reaction rate of the reactant on the electrode surface is described by the Butler-Volmer equation:

$$-D\left.\frac{\partial c}{\partial n}\right|_{surf} = -k_0 exp\left(\frac{\beta F(E-E_f)}{RT}\right)c_{surf} + k_0 exp\left(-\frac{\alpha F(E-E_f)}{RT}\right)(1-c_{surf}) \qquad (S2)$$

where k_0 is the standard heterogeneous rate constant. α and β are transfer coefficients and $\alpha + \beta = 1$. For the fully irreversible case, k_0 is selected to be a small value compared to the diffusion rate D/r_{el} ($k_0 < 0.01D/r_{el}$) and both α and β are selected to be 0.5 (in fact, for the fully irreversible condition, any change of the values of α, β and k_0 will not influence the peak current ratios). As shown in Fig. S5, the transition from the radial diffusion where the reaction is significantly affected by the geometry to the linear diffusion where the reaction is mainly determined by the electroactive surface area rather than the exact geometry is also found for an irreversible one-electron-transfer reaction.

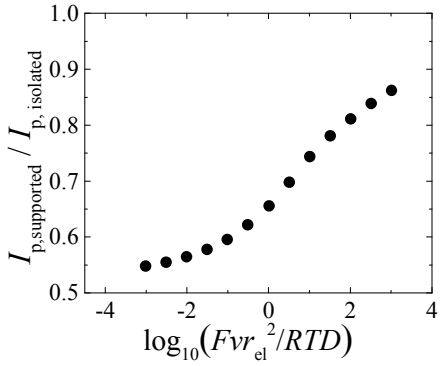

Figure S5: The $I_{p,supported}$ / $I_{p,isolated}$ ratios for irreversible one-electron transfer process at different Fr_{el}^2v/RTD.

Table S3: The $I_{p,supported}$ / $I_{p,isolated}$ ratios for irreversible one-electron transfer process at different Fr_{el}^2v/RTD

$\log_{10}(Fr_{el}^2v/RTD)$	$I_{p,supported}$ /$I_{p,isolated}$
-3.01	0.548
-2.51	0.555
-2.01	0.565
-1.51	0.578
-1.01	0.596
-0.51	0.622
0.01	0.656
0.51	0.698
1.01	0.744
1.51	0.781
2.01	0.811
2.51	0.839
3.01	0.862

S 2.3 Reproducibility of electrodes

The reproducibility of the voltammetric responses at the supported microwires is reported in Section 4.3 of the main text to be 0.6% and 4.6% within the electrode and between electrodes respectively. The voltammograms are provided in Figure S6 below.

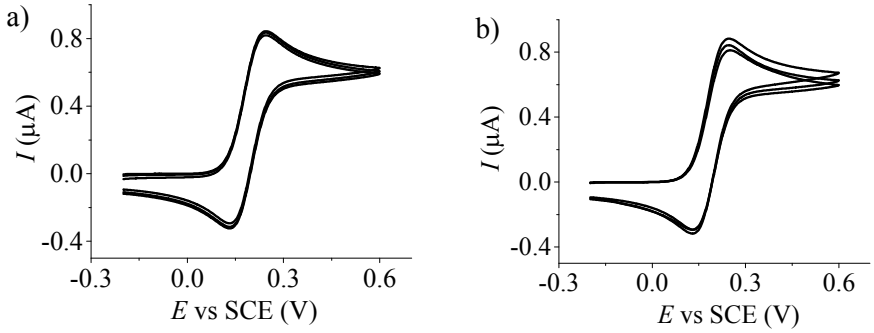

Figure S6: Cyclic voltammetry of 1.0 mM $FcCH_2OH$ oxidation in 0.1 M KCl at the supported microwire electrodes at the scan rate of 100 mV s^{-1}, 298 K; a) same electrode, multiple scans; b) different electrodes

S 2.4 GSH measurements

The concentration of GSH is determined by the reaction with excess DTNB to form TNB. TNB is then detected by amperometric measurements of TNB oxidation, which is first

characterized for its electron transfer coefficient (β) and diffusion coefficient (D) using cyclic voltammetry at a glassy carbon macro-electrode (GC), discussed below.

S 2.4.1 Preliminary studies of TNB oxidation

Cyclic voltammetry of 0.84 mM TNB oxidation is performed at a GC (r_e = 1.49 ± 0.02 cm) at 298 K at the scan rates of 25, 50, 100, 200, 300 and 400 mV s^{-1}. The voltammograms are presented in Figure S7a and the peak currents plotted against the square root of scan rates in Figure S7b. The voltammograms obtained are subjected to Tafel analysis[1] giving the value of transfer coefficient (β) of 0.24. The diffusion coefficient (D) is then determined using eqn. S3[1] to be 1.36 x 10^{-9} ± 0.04 x 10^{-9} m^2 s^{-1}.

$$I_p = 0.496\sqrt{\alpha}FA_e c^* \sqrt{\frac{FD\nu}{RT}} \qquad \text{(S3)}$$

where I_p is the peak current. α, F, A_e, ν, R, T, $c^*$and D are the transfer coefficient, Faraday constant (96,485 C mol^{-1}), electrode surface area, scan rate, molar gas constant (8.314 J K^{-1} mol^{-1}), absolute temperature and bulk concentration and diffusion coefficient of the redox-active species, respectively.

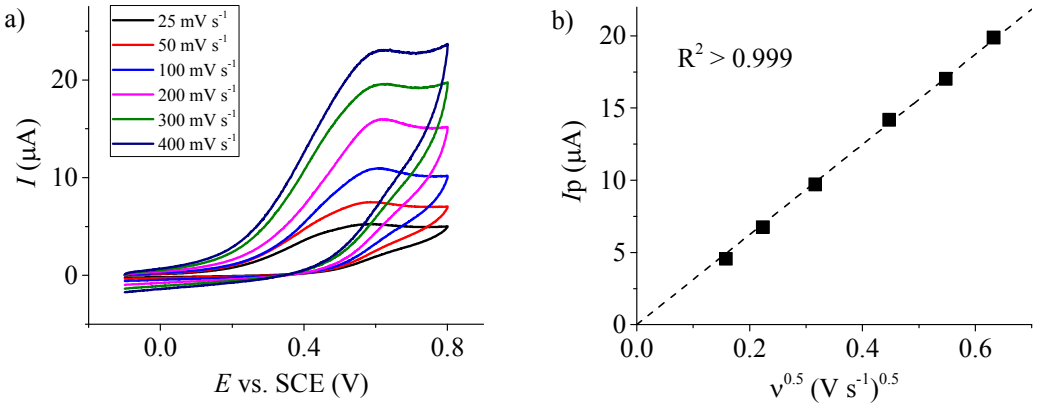

Figure S7: a) Cyclic voltammetry of 0.84 mM TNB oxidation at GC electrode at the scan rates of 25, 50, 100, 200, 300 and 400 mV s^{-1}; b) Voltammetric peak currents as a function of square root of scan rates.

Similar experiments were performed at the supported microwire electrode. The value of transfer coefficient (β) of TNB oxidation at the wire electrodes was determined to be 0.26, similar to the value obtained at the glassy carbon and that previously reported in literature.[2]

S 2.4.2 Enhanced sensitivity

Figure 6 (main text) displays the cyclic voltammograms of 168 μM TNB oxidation at different carbon electrodes having different ratios of Faradaic to capacitative currents (i_F/i_C). The measurements of the i_F/i_C ratios are detailed below.

- **Non-Faradaic contribution**

Capacitance of the electrodes is measured by cyclic voltammetry of blank electrolyte (0.1 M pH 7.5 phosphate buffer, 10 mM EDTA) at the scan rate of 25 mV s^{-1}. The resulting amperometric current is due to the build-up of charge at the electrode surface. The capacitative current (i_C) is measured at 0.7 V vs. Ag. At the same time, cyclic voltammetry of the oxidation of 168 μM TNB in 0.1 M phosphate buffer pH 7.5 at the scan rate of 25 mV s^{-1} is performed and the value of its peak current (i_F) at 0.7 V vs. Ag is noted. The ratios of Faradaic to capacitative currents (i_F/i_C) are then determined, and the resulting values given in Fig. 6 (main text).

- **Carbon microdisk electrode**

It is discussed in the main text that the commercial microdisk electrodes have capacitance much larger than predicted for its geometric area, likely reflecting the imperfect sealing of the electrodes and the occurrence of cracks potentially from the manufacturing processes. To confirm that this is the case, the cyclic voltammogram provided by the supplier is given in Fig. S8 below to show that the capacitance observed is of similar level as the newly manufactured electrode (1977 ± 441 μF cm^{-2}).[3]

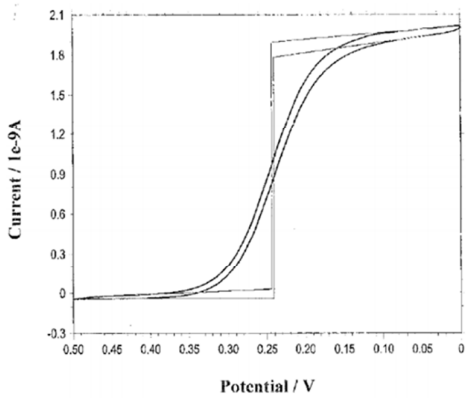

Figure S8: Cyclic voltammogram of 2 mM $K_3Fe(CN)_6$ in 1 M KNO_3 measured at the scan rate of 0.2 V s^{-1} at a commercial microdisk electrode with a radius of 3.5 μm. This image is provided by the supplier along with commercial electrode.

S 2.4.3 Calibration curve

The concentration of GSH is determined by the reaction with excess DTNB to form TNB. TNB is then detected by amperometric measurements. In the main text, the detection of TNB using cyclic voltammetry is discussed in detail. In this Supporting Information, we will focus on the measurement of TNB using chronoamperometry.

An excess amount of DTNB (168 μM) was used to react with 0, 5, 10, 20, 30, 45 and 65 μM of GSH in 0.1 M, pH 7.5 phosphate buffer in the presence of 10 mM ethylene-diaminetetraacetic acid (EDTA; to prevent GSH oxidation catalyzed by metal ions impurity in the solutions[4]). The mixtures were left to react for 2 minutes to allow the reactions to go to completion, and hence produce 0, 5, 10, 20, 30, 45 and 65 μM of TNB. Chronoamperometry was performed to the reaction mixtures by applying the potential of 0.75 V vs. Ag wire for 10 s. The amperograms obtained and the calibration plot of the steady state currents taken at 10 s against GSH concentrations are given in Fig. S9. The sensitivity of the measurement is 0.7 nA μM^{-1}, and the limit of detection determined to be 1.3 μM ($3s_B/m$).

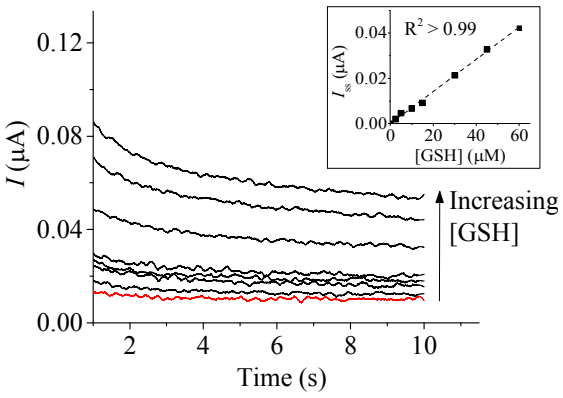

Figure S9: (Black) Chronoamperometry of 0, 5, 10, 20, 30, 45 and 65 μM of GSH reacted with 168 μM DTNB for 2 min to form equal concentrations of TNB at the supported microwire electrode. (Red) Blank electrolyte solution. ν = 25 mV s^{-1}. 298 K. Inlay: calibration plot of quasi-steady state currents (I (t = 10 s)) against GSH concentration.

References

(1) Compton, R. G.; Banks, C. E. *Understanding Voltammetry*, 2nd ed.; Imperial College Press, 2011, p 444.

(2) Nekrassova, O.; Lawrence, N. S.; Compton, R. G. *Electroanalysis* **2003**, *15*, 1501-1505.

(3) Cinková, K.; Clark, M.; Sokolov, S. V.; Batchelor-McAuley, C.; Švorc, Ľ.; Compton, R. G. *Electroanalysis* **2016**.

(4) Ngamchuea, K.; Batchelor-McAuley, C.; Compton, R. G. *Chemistry - A European Journal* **2016**, *22*, 15937-15944.